Volume 5
Number 24
21 December 2023
Pages 6739–7090

Nanoscale Advances

rsc.li/nanoscale-advances

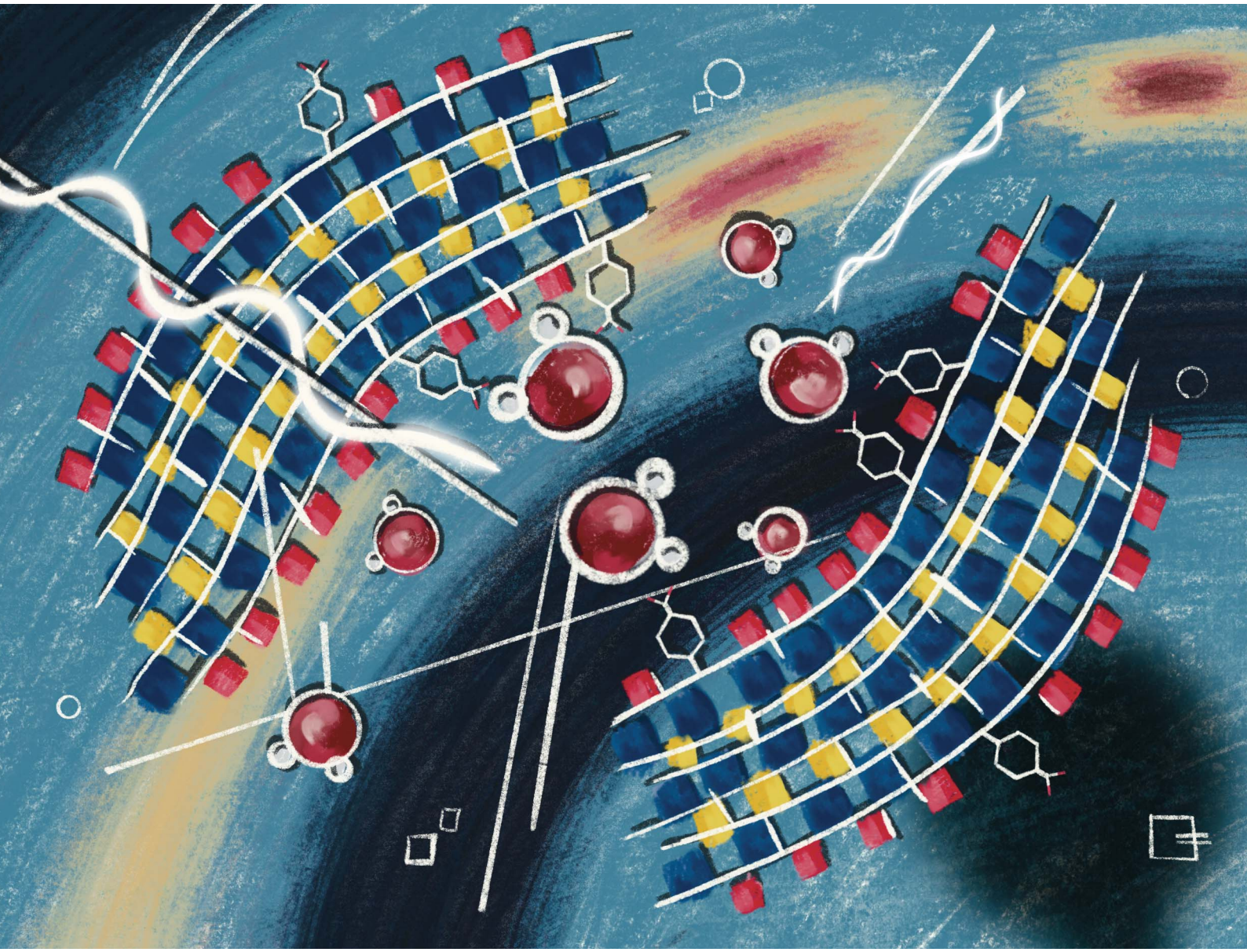

ISSN 2516-0230

ROYAL SOCIETY OF CHEMISTRY

PAPER

Elena Miliutina *et al.*

Plasmon assisted $Ti_3C_2T_x$ grafting and surface termination tuning for enhancement of flake stability and humidity sensing performance

NCNST

Nanoscale Advances

ROYAL SOCIETY OF CHEMISTRY

PAPER

View Article Online
View Journal | View Issue

Cite this: *Nanoscale Adv.*, 2023, **5**, 6837

Plasmon assisted $Ti_3C_2T_x$ grafting and surface termination tuning for enhancement of flake stability and humidity sensing performance†

Vladislav Buravets,[a] Anastasiia Olshtrem,[a] Vasilii Burtsev,[a] Oleg Gorin,[a] Sergii Chertopalov,[b] Andrei Chumakov,[c] Matthias Schwartzkopf,[c] Jan Lancok,[b] Vaclav Svorcik,[a] Oleksiy Lyutakov[a] and Elena Miliutina *[a]

Humidity sensors play a critical role in monitoring human activities, environmental health, food processing and storage, and many other fields. Recently, some 2D materials, particularly MXenes, have been considered as promising candidates for creating humidity sensors because of their high surface area, surface-to-bulk ratio, and excellent conductivity, arising from the high concentration and mobility of free electrons. In this work, we propose the plasmon-assisted surface modification and termination tuning of common MXene ($Ti_3C_2T_x$) to enhance their response to humidity and increase their stability against oxidation. Hydrophobic ($-C_6H_4-CF_3$) and hydrophilic ($-C_6H_4-COOH$) chemical moieties were covalently grafted to the $Ti_3C_2T_x$ surface using plasmon-mediated diazonium chemistry. *In situ* Grazing-Incidence Wide-Angle X-ray Scattering (GIWAXS) measurements, performed at different humidity levels indicate that surface modification significantly affects penetration of water molecules in $Ti_3C_2T_x$ films. As a result, the sensitivity of the flakes to the presence of water molecules was significantly altered. Additionally, proposed surface grafting commonly proceeds on the less stable MXene surface sites, where flake oxidation commonly initiates. As a result of the modification, such "weak" and more chemically active sites were blocked and $Ti_3C_2T_x$ stability was significantly enhanced.

Received 19th June 2023
Accepted 19th September 2023

DOI: 10.1039/d3na00429e

rsc.li/nanoscale-advances

Introduction

Humidity sensors are important for monitoring human activities, environmental changes, food processing, and health issues.[1,2] The general requirements for active materials in such sensors (and corresponding materials) include high sensitivity to moisture presence, wide detection range, quick response, low cost and scalable/reproducible preparation route.[3,4] Among the related materials, those with 2D structure are considered the best candidates, due to their unique surface-to-volume ratio and related sensitivity to the external environment.[5–7] An additional requirement for 2D materials is a sufficient density of electrons with high mobility to ensure a rapid and intense response to moisture presence. Discovered by Gogotsi's group in 2011 MXene(s) satisfy almost all of the abovementioned requirements.[8,9] For instance, the $Ti_3C_2T_x$ flakes (which represent the most investigated MXene) have a high concentration of free electrons with high mobility, in addition to their 2D structure and, consequently, high sensitivity to the external environment.[10–12] Despite the fact that MXenes have no bulk counterparts as minerals in nature, like some other 2D materials,[13] they are composed of common elements and can be mass-produced. This should also be an important factor in the production of low-cost humidity sensors. An additional advantage of MXenes is that their internal properties and interactions with the external environment, can be controlled by changing the flakes surface termination.[14] Thus, the utilization of MXene flakes and thin films based on them for the creation of humidity and other sensors has been widely reported.[15–17] It has been demonstrated that even small amount of hydration leads to a significant increase of the interlayer spacing in the structure of MXene-based films causing significant decrease in conductivity, which can be monitored by simple resistivity measurements.[18–20]

On the other hand, involvement of MXenes as the sensor's active material actually meets two significant drawbacks: (i) – unsatisfactory preparative reproducibility and (ii) – weak stability under the operation conditions.[21,22] Specifically, the surface termination of MXene flakes is a strong function of etching/delamination conditions and can vary significantly with even slight changes in the experimental procedures for flake preparation.[10,23,24] Since the MXene–water interaction is determined by the

[a]*Department of Solid State Engineering, University of Chemistry and Technology, 16628 Prague, Czech Republic. E-mail: elena.miliutina@vscht.cz*

[b]*Institute of Physics of the Czech Academy of Sciences, Na Slovance 1999/2, 18200 Prague, Czech Republic*

[c]*Deutsches Elektronen-Synchrotron DESY, 22607 Hamburg, Notkestr. 85, Germany*

† Electronic supplementary information (ESI) available. See DOI: https://doi.org/10.1039/d3na00429e

surface terminations, the response of the MXene-based sensors can significantly deviate due to slight deviations in flakes' preparation (and different surface termination). Another unresolved question of MXenes utilization (in particular, using of $Ti_3C_2T_x$ flakes) is their low stability.[22,25] Exposure of $Ti_3C_2T_x$ flakes to ambient atmosphere with humidity levels of approximately 20–30% leads to oxidation of the flake with formation of wide bandgap TiO_2 and subsequent loss of materials functionality.[26,27] The oxidation commonly starts at the flake edges or "weak" sites of basal plane (defects or –OH terminated titanium atoms) and then spreads across the entire flake surface.[28–30] To prevent flake oxidation (or at least minimize its impact), approaches combining flakes with different materials to "block" the "weak" sites in flakes surface have been proposed.[31–34] Such surface blocking can be reached through the MXenes surface modification and related changes in the termination of flakes. Commonly, high energy treatments, such as temperature annealing or plasma processing, are used to tune the surface chemistry of MXenes.[10,35–37] However, such rough methods can damage the MXenes structure and lead to a loss of functionality of the flakes. As an alternative, few chemical approaches capable of changing the flakes surface composition were proposed. Most of them utilize the noncovalent interaction of MXenes flakes (using, for example, hydrogen-binding or electrostatic interactions) with various organic small molecules or polymers.[38–43] Such approaches are favored by their simplicity, but the stability of the surface functionalization (especially under different operating conditions) can be low. As an alternative, covalent functionalization of MXenes with the formation of strong bonds between the flakes and grafted organic moieties has been proposed. Commonly, covalent approaches are based on the utilization of diazonium chemistry or silanization of the surface-terminated oxygen group.[44–48] Such approaches can significantly enhance the flakes stability and expand their utilization potential.

Recently, we demonstrated that utilization of plasmon-assisted chemistry can modify the surface termination of MXene flakes, significantly enhancing their stability as well as tune their polarity.[49,50] Our approach is based on the plasmon-assisted decomposition of organic salts, with formation of highly reactive radicals, which promptly graft to the nearby solid surface.[49–51] The grafting takes place at chemically active sites within the MXene flakes' structure ensuring the stability enhancement. Resulted surface terminations are determined by the chemical structure of used organic salts, thereby compensating for uncertainties in the flakes surface terminations that can arise during the MXene etching/delamination processes.

In this work, we demonstrated the advantages of plasmon-assisted MXene surface modification for tuning the interaction of $Ti_3C_2T_x$ flakes with water molecules, enhancing their sensitivity towards specific humidity levels and prolonging the lifetime of MXenes under operating conditions.

Experimental

Detailed description of samples preparation and characterization is given in ESI.† Briefly, $Ti_3C_2T_x$ flakes were prepared by etching and subsequent delamination of the corresponding Ti_3AlC_2 MAX phase. Surface modification of $Ti_3C_2T_x$ flakes was performed by mixing flakes with the corresponding solution of arenediazonium tosylate salts (ADT) and illumination with light emitting diode (LED, 780 nm), with emission wavelength, corresponded to the excitation of $Ti_3C_2T_x$ surface plasmon. Flakes were grafted by hydrophobic ($-C_6H_4-CF_3$) and hydrophilic chemical moieties ($-C_6H_4-COOH$). In the next step, thin films (thickness $\approx$ 2 μm) were prepared by drop deposition of flakes on the flexible polypropylene membrane (for sensor application) or on Si substrate (for control measurements).

In situ water penetration tests and resistance measurements at Grazing-Incidence Wide-Angle X-ray Scattering (GIWAXS) were performed at P03 beamline PETRA III (DESY), using specially designed humidity cell.[52,53] MXene films response to humidity was analyzed as a function of external humidity using two-contact resistance measurement. The amounts of entrapped water were additionally analyzed by Quartz Crystal Microbalance technique (resonance frequency – 10 MHz).

Results and discussion

$Ti_3C_2T_x$ flake's surface modification and termination tuning is schematically presented in Fig. 1A and S1.† Surface grafting was performed using two types of chemical moieties with "opposite" behavior toward water – hydrophobic ($-C_6H_4-CF_3$) and hydrophilic ($-C_6H_4-COOH$) chemical moieties were grafted to flakes surface with utilization of plasmon assisted chemistry (grafted MXene flakes are further refereed as Ti_3C_2–COOH and Ti_3C_2–CF_3). In the proposed experimental concept, the $Ti_3C_2T_x$ suspension and ADT solution were mixed together and subjected to illumination with wavelength corresponding to the excitation of MXene's plasmon resonance at 800 nm (Fig. S2†). The ADT-related organic cations were electrostatically absorbed on the flake's surface (Fig. S1†) and subjected to high-energy plasmonic field. As a result of plasmon triggering the organic cations split off the nitrogen molecule with the creation of highly reactive radicals. Produced radicals were immediately grafted to nearby surface, *i.e.* to $Ti_3C_2T_x$ flakes. As was reported previously, the grafting proceeds at the more "reactive" surface sites – flake's edges, –OH terminated groups (Fig. S3† reveals the apparent decrease of characteristic –OH band intensity) and defects on the flake's basal planes (Fig. S1†).[34,49,50] The $Ti_3C_2T_x$ surface modification proceeds solely under the plasmon-assisted chemistry (*i.e.* under illumination with wavelength, corresponding to the excitation of surface plasmon on $Ti_3C_2T_x$ flakes), which was indicated by control measurements (Fig. S2 and S4†).

Proofs of surface modification

The grafting of $Ti_3C_2T_x$ flakes with organic moieties was confirmed using Surface-Enhanced Raman Spectroscopy (SERS) (Fig. 1B). SERS spectra of pristine and grafted flakes reveal the characteristic bands, located in the range between 100 and 800 cm^{-1} – modes at 206 and 731 cm^{-1} correspond to the out-of-plane vibrations of A_{1g} symmetry of $Ti_3C_2T_x$, while peaks at 260, 285, 364, 515, 618 and 662 cm^{-1} are consistent with the E_g

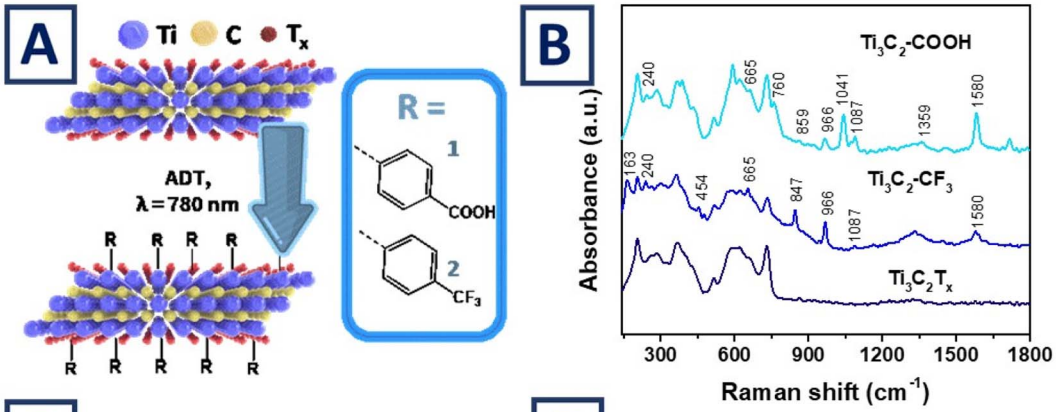

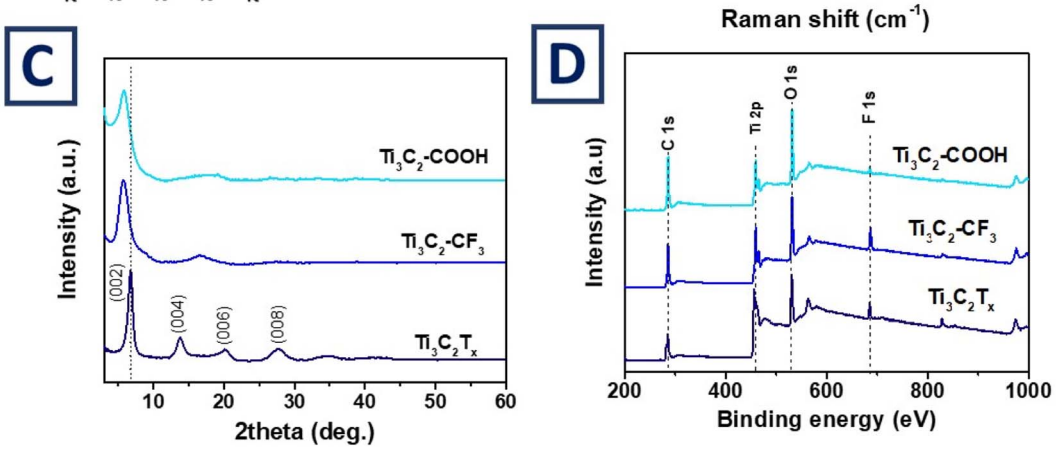

E

Name of sample	Surface atom element concentration (% at.)			
	Ti 2p	O 1s	C 1s	F 1s
$Ti_3C_2T_x$	28.2	26.2	38.2	7.4
Ti_3C_2-CF_3	14.4	28.9	46.3	10.4
Ti_3C_2-COOH	11.7	33.1	53.1	2.1

Fig. 1 (A) Plasmon-assisted MXene surface grafting with hydrophilic (–C_6H_4–COOH) or hydrophobic (–C_6H_4–CF_3) chemical moieties; (B) SERS spectra of pristine $Ti_3C_2T_x$ flakes and flakes grafted with –C_6H_4–COOH and –C_6H_4–CF_3 chemical moieties (spectral positions of new appeared bands are highlighted); (C) XRD patterns of pristine and grafted flakes; (D) survey XPS spectra of pristine and grafted $Ti_3C_2T_x$ flakes; (E) evaluated from XPS surface elemental composition of pristine and grafted $Ti_3C_2T_x$ flakes.

modes and the vibrations of the termination groups.[54] These peaks are slightly changed after $Ti_3C_2T_x$ surface modification. Notably, appearance of the additional SERS peaks, corresponding to benzene ring vibration and –COOH/–CF_3 vibration bands, are well visible after the flake grafting. These peaks are designated in Fig. 1B and correspond well with the chemical structure of grafted organic moieties (peak assignment is given in Table S1†). In addition, the characteristic vibration of A_{1g} modes of $Ti_3C_2T_x$ were also affected by the change of the flake's surface termination, similarly to the previously reported findings.[54]

X-ray diffraction (XRD) patterns[55] of pristine and grafted flakes are presented in Fig. 1C. As expected, characteristic reflexes of Ti_3C_2 for (002), (004), (006) and (008) planes are well observed in the pattern of pristine $Ti_3C_2T_x$ flakes. The absence of the peak at 39.3° confirms that Al layers were completely etched from the initial Ti_3AlC_2 MAX phase.[56] After modification, the low-angle XRD peak (002) is apparently shifted to a lower value, indicating an increase in the flake interlayer distance, likely due to steric effects. Specifically, it was found that interplanar distance corresponded to 13.06 Å for $Ti_3C_2T_x$ and expanded to 15.18 and 15.32 Å for –C_6H_4–CF_3 and –C_6H_4–COOH surface grafting, respectively. Furthermore, XRD patterns also indicate the weakening (almost complete disappearance) of (004), (006) and (008) peaks after the flake grafting. Such phenomenon can be attributed to less densely packed structure of flake films (*i.e.*, interplanar distance increase) and related changes of angular or absorption factors of X-ray diffraction.[57]

Survey X-ray photoelectron spectroscopy (XPS) spectra are presented in Fig. 1D and corresponding table – see part D of Fig. 2. As can be expected the MXene surface composition is presented mainly by the Ti, C, F and O elements. Following the

modification, the characteristic Ti peak is attenuated due to the screening by the grafted organic moieties. Simultaneously, the apparent increased in the C(1s) peak intensity was observed, indicating the increase of carbon surface concentration. Furthermore, the grafting with $-C_6H_4-CF_3$ led to an increase in the F surface concentration, while the grafting with $-C_6H_4-COOH$ in an increase in the oxygen concentration. Thus, the observed changes of surface composition also indicate the successful grafting of $Ti_3C_2T_x$ flakes with corresponding chemical moieties, correlating well with SERS results. Significantly, appearance of characteristic nitrogen peaks on XPS graphs was not observed, further confirming that the proposed grafting proceeds through the release of N_2 molecules, radical production, and formation of stable covalent bonds between flakes' surface and grafted organic moieties (Fig. S1†). Lastly, water contact angle (CA) measurements were performed on the MXene thin film surface in order to illuminate the impact of termination tuning. Results of wettability tests (Fig. S5†) indicate the apparent decrease of water CA on Ti_3C_2–COOH surface (CA = 16°) and its increase on Ti_3C_2–CF_3 surface (CA = 80°) in comparison with pristine $Ti_3C_2T_x$ flakes (CA = 52°).

In the next step we fabricated sensor structures with thin MXene films (as an active material) on PP (polypropylene) membrane. To connect sensors to the circuit two gold contacts were sputtered on the opposite edge sides of the MXene films (contact lengths – 15 mm, distance between contacts – 15 mm). Photos of as-prepared and bent $Ti_3C_2T_x$/PP films are given in Fig. 2A, revealing the good quality and flexibility of the created structures. To further explore quality of the pristine and modified MXene-based sensors scanning electron microscopy (SEM) imaging and energy-dispersive X-ray spectroscopy (EDX) analysis of MXene films' cross-section were performed (Fig. 2B–D). As is evident, a $Ti_3C_2T_x$ based films with homogeneous structure were created from all, pristine and grafted flakes. The EDX mapping also confirms the homogeneous distribution of flakes (Ti mapping) and grafted organic moieties (F and O mapping). Thickness of the $Ti_3C_2T_x$ based films was estimated from cross-section SEM images and found to be near 2 μm (procedure was optimized to obtain the same thickness for the films based on $Ti_3C_2T_x$, Ti_3C_2–COOH and Ti_3C_2–CF_3 films and thereby eliminate the effect of thickness on the response of the created humidity sensor).

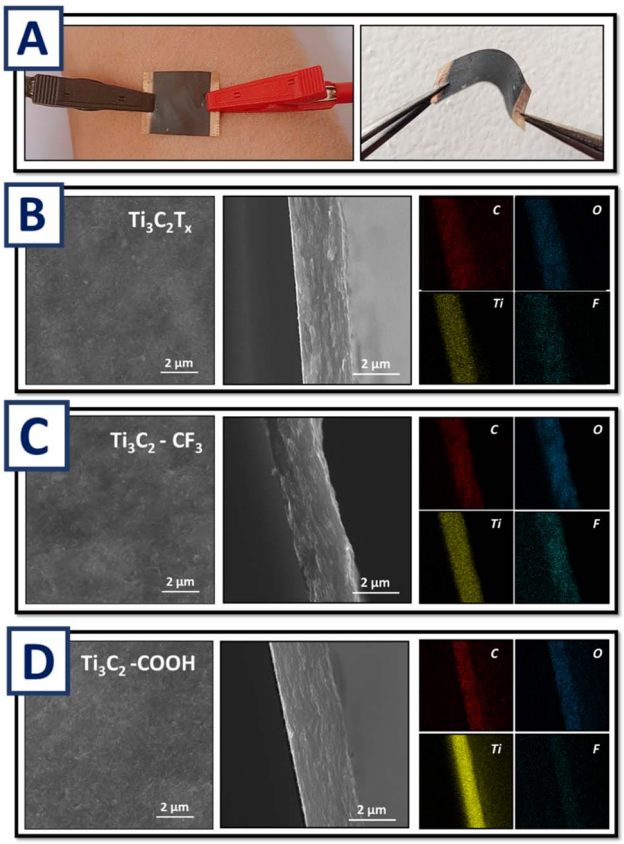

Fig. 2 (A) Photos of created humidity sensors based on pristine or grafted $Ti_3C_2T_x$ flakes deposited on flexible PP membrane; (B)–(D) SEM images and corresponded EDX mapping of thin films created from pristine $Ti_3C_2T_x$ flakes and flakes grafted with $-C_6H_4-COOH$ and $-C_6H_4-CF_3$ flakes.

Humidity sensing

The pristine and grafted $Ti_3C_2T_x$ thin films were subsequently tested for humidity sensing. Experiments were performed in two-electrode mode by monitoring current changes (in particular – thin films conductivity changes) as a function of the humidity level. Samples were cyclically exposed to various humidity levels, left to regenerate (at zero humidity level) and subjected again to another (lower) level of humidity. Relative changes of normalized currents (measured in chronoammetry mode under 10 mV external bias) are presented in Fig. 3 as a function of humidity level and flakes surface termination. As evident, the presence of humidity leads to resistivity increase and, consequently, decrease of electric current flowing between the gold electrodes. The response of MXene films revealed strong dependence on the surface modification. In the case of pristine $Ti_3C_2T_x$ films poorly pronounced current changes were observed as the humidity increased from zero to 10% level, rapid current decrease with subsequent increase of humidity levels to 80% and less significant changes of films conductivity in the 80–100% humidity range (Fig. 3A). A distinct response to the presence of moisture was observed for flakes grafted with $-C_6H_4-COOH$ chemical moieties (Fig. 3B). For this modification, significant current decrease was observed even at low humidity levels (below 10%). With a subsequent humidity increase, the saturation of sensor was reached and the Ti_3C_2–COOH flakes response was less pronounced. The opposite response was observed for flakes grafted with hydrophobic $-C_6H_4-CF_3$ chemical moieties. The conductivity of Ti_3C_2–CF_3 films was almost unaffected in presence of low humidity concentrations. However, for high humidity values (exceeding 50%), a rather sharp drop in current was observed with subsequent decrease as the humidity concentration increase. As evident, the proposed surface termination tuning makes it possible to significantly increase the response of MXene flakes toward particular humidity level – grafting by hydrophilic –COOH groups allows to increase the sensitivity of the material at low

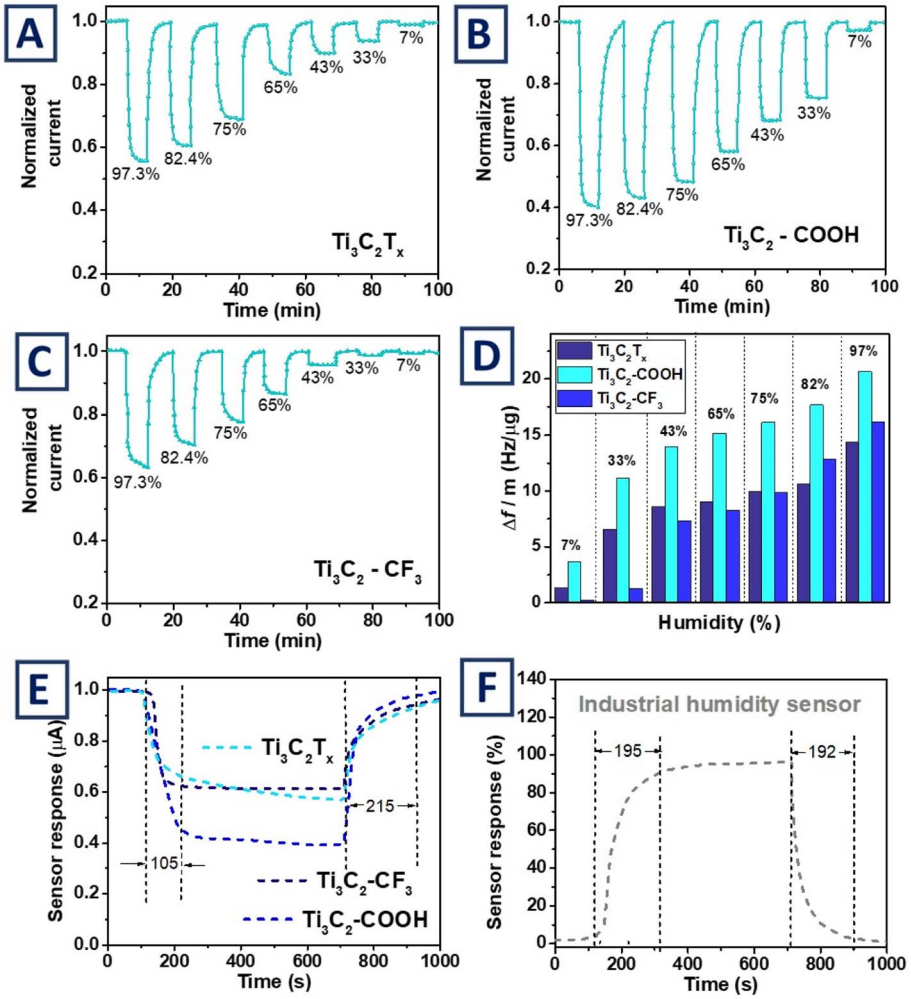

Fig. 3 (A)–(C) Cyclic response of pristine and grafted $Ti_3C_2T_x$ films conductivity to different humidity levels (from high to low), measured as a function of normalized value of electric current in two-electrode system; (D) water molecules entrapment by pristine or grafted MXene films, measured by resonant frequency shift (normalized per MXene mass) of quartz-crystal with top-deposited thin $Ti_3C_2T_x$ layer; (E) time-resolved changes of pristine and grafted $Ti_3C_2T_x$ flakes conductivity to rapid humidity increase, for comparison the response of the commercial sensor is presented in (F).

humidity values, while modification with hydrophobic $-CF_3$ chemical moieties, on the contrary, shifts the sensor sensitivity to higher humidity values.

In general, the observed behavior correlates well with the surface modification of MXene flakes and with the proposed humidity response mechanism, which is based on the sorption of water molecules, an increase in the flake's interlayer distance and, accordingly, hindering of the electron transport in $Ti_3C_2T_x$ film(s). Pristine flakes contain both hydrophilic (= O, –OH) and hydrophobic (–F) termination groups, which makes it possible to achieve the water entrapping and humidity detection at various moisture levels. Replacing surface termination with hydrophilic groups results in easier entrapment of water molecules, making the Ti_3C_2–COOH flakes more sensitive to low humidity levels. In turn, hydrophobization of the flake's surface prevents the entrapment of water molecules. Thus, Ti_3C_2–CF_3 films are insensitive to relatively low humidity, but show good response when the sorption resistance barrier is overcome by the increased humidity level.

Dependence of the water molecules entrapment on surface modification of MXene was further investigated by means of quartz crystal microbalance experiment, following shift of a resonant frequency of piezo crystal with deposited $Ti_3C_2T_x$ layer in presence of various humidity levels (flakes were deposited using drop casting method, average thickness – *ca* 2 μm). The experiments were carried out for the original and grafted $Ti_3C_2T_x$ films and the results obtained are presented in Fig. 3D (the normalized shift of the quartz-crystal resonance frequency is associated with a mass increase of investigated film due to water molecules entrapment). As is evident, the pristine $Ti_3C_2T_x$ film captures water molecules in the entire range of humidity. In turn, the entrapment of water molecules by Ti_3C_2–CF_3 thin films was insignificant for low humidity values, up to 33%. However, these flakes were able to efficiently entrap water at higher humidity levels. The

normalized shift (per mass of MXene) of the resonant frequency was almost the same for the pristine and hydrophobic Ti_3C_2–CF_3 films, at the humidity level near 100%. In turn, entrapment of the water molecules by hydrophilic Ti_3C_2–COOH was especially pronounced at low humidity levels. A sharp shift of the resonant frequency was observed in the humidity range of 0–50%. Thus, mass changes of the MXene films measured with quartz-crystal microbalance generally confirmed our previous experiments – the original MXene entraps water relatively efficiently in the entire humidity range. The hydrophilic Ti_3C_2–COOH was very efficient for water entrapment at low moisture levels, making this material efficient for the detection of low humidity. The hydrophobic Ti_3C_2–CF_3 film does not capture water in the low humidity ranges but captures water at high moisture concentrations, making this material efficient for monitoring of the high humidity levels.

We also evaluated the response time of pristine and grafted $Ti_3C_2T_x$ flakes to rapid humidity increase (Fig. 3E). The obtained results were compared with commercial humidity sensor response. As is evident, the response time of $Ti_3C_2T_x$ flakes was almost not affected by flakes surface grafting. Moreover, pristine and grafted flakes show quicker response than the commercial sensor – the saturation of sensor response is reached in 105 seconds for MXene films *vs.* 195 s for the commercially available sensor (Fig. 3F). The relaxation time of the commercial sensor was shorter than in the case of MXene films. However, in this case the difference was less significant – the commercial sensor completely relaxed within 192 s, while the MXene films – within 215 s. Lastly, it should be also noted that all current/humidity experiments were performed by applying only 10 mV, indicating that proposed sensors can be potentially powered by low-energy sources, such as solar, tribo- or piezo-generated energy.[58,59]

Time-resolved GIWAXS measurements

To further check the water molecules intercalation and corresponding flakes' interlayer distance changes, we performed *in situ* GIWAXS analysis at variable humidity levels. For this purpose, pristine and grafted $Ti_3C_2T_x$ films were placed in the humidity chamber and stabilized at set humidity for approximately 10 minutes before conducting measurements (Fig. 4A and S6†). Noteworthy, *in situ* GIWAXS measurements were performed, with particular focus on low-angle peak position, reflecting changes of (002) plane due to penetration of water molecules in the space between flakes. The positions of (002) peak for all flakes were found to be a function of external humidity (Fig. 4B–D), with the shift extent determined by flakes' surface termination. In the case of pristine $Ti_3C_2T_x$ flakes the (002) peak is continuously shifting with gradual increase of humidity. In the case of Ti_3C_2–CF_3 films, the (002) peak stays at its initial position at low humidity levels and shifts significantly at high humidity values. In the case of Ti_3C_2–COOH films, the opposite situation was observed, (002) peak shifts significantly under the appearance of low moisture concentration, while further peak shift with subsequent increasing of humidity level is less pronounced. The *d*-spacing of $Ti_3C_2T_x$ films was calculated from GIWAXS measurements and compared with the corresponding changes in conductivity at different humidity levels (Fig. 4E–G). As is evident, the shapes of obtained curves perfectly correlate with the assumption that entrapment of water molecules led to the increase of the distance between flakes, which, in turn, hinders charge transfer and reduces the conductivity of thin films. Thus, the results of the *in situ* GIWAXS measurements additionally highlight the impact of flakes' surface termination tuning for the entrapment of water molecules. While pristine $Ti_3C_2T_x$ flakes are able to entrap water molecules in wide range of humidity levels with consistent efficiency, surface modification with –COOH chemical moieties facilitates entrapment of the water molecules at low humidity level, and the surface modification with hydrophobic –CF_3 chemical moieties prevents the water molecules entrapment at low humidity level, but enhances sensitivity at higher humidity levels. Consequently, performed *in situ* GIWAXS experiments clearly indicate that water molecules entrapment is a function of MXene surface modification.

Stability of films in operando conditions

Finally, the sensors' stability performance was evaluated. As was reported earlier, the $Ti_3C_2T_x$ flakes tend to degrade with the formation of TiO_2 and carbon residues. This process is especially quick in the presence of oxygen and moisture. However, the proposed route of $Ti_3C_2T_x$ surface modification can block the "weaker" sites of the flake's surface (edges, defects or –OH terminated groups) preventing the initial stage of degradation and thus increasing flakes' stability. Conductivity of the MXene-based thin films, measured before and after storage at ambient conditions (with corresponding "natural" deviation of surrounding temperature and humidity) is presented in Fig. 5A. As can be expected, storage of pristine $Ti_3C_2T_x$ film for long-time period led to significant decrease of materials conductivity (Fig. 5A). This phenomenon is also accompanied by complete loss of material's functionality – response to humidity changes were no more observed on aged pristine-based $Ti_3C_2T_x$ film. For the film based on Ti_3C_2–CF_3 but storage-induced conductivity decrease was also detected, but to a significantly less extent. Finally, almost complete conservation of thin film conductivity was observed for MXene protected by –COOH grafting (Fig. 5A). The prevention of flakes degradation and preservation of $Ti_3C_2T_x$ chemical structures also made it possible to largely preserve the functionality of material and extend its lifez time (Fig. 5B). In particular, the stored Ti_3C_2–COOH shows almost the same response as before storage, however, slight deceleration of thin films was observed. More significant deterioration in sensitivity was observed for Ti_3C_2–CF_3, but, unlike aged ungrafted MXene, its response to the presence of moisture was still observable. Subsequently performed XPS measurements (Fig. 5C) reveal that sensor functionality decrease correlates with flakes oxidation and

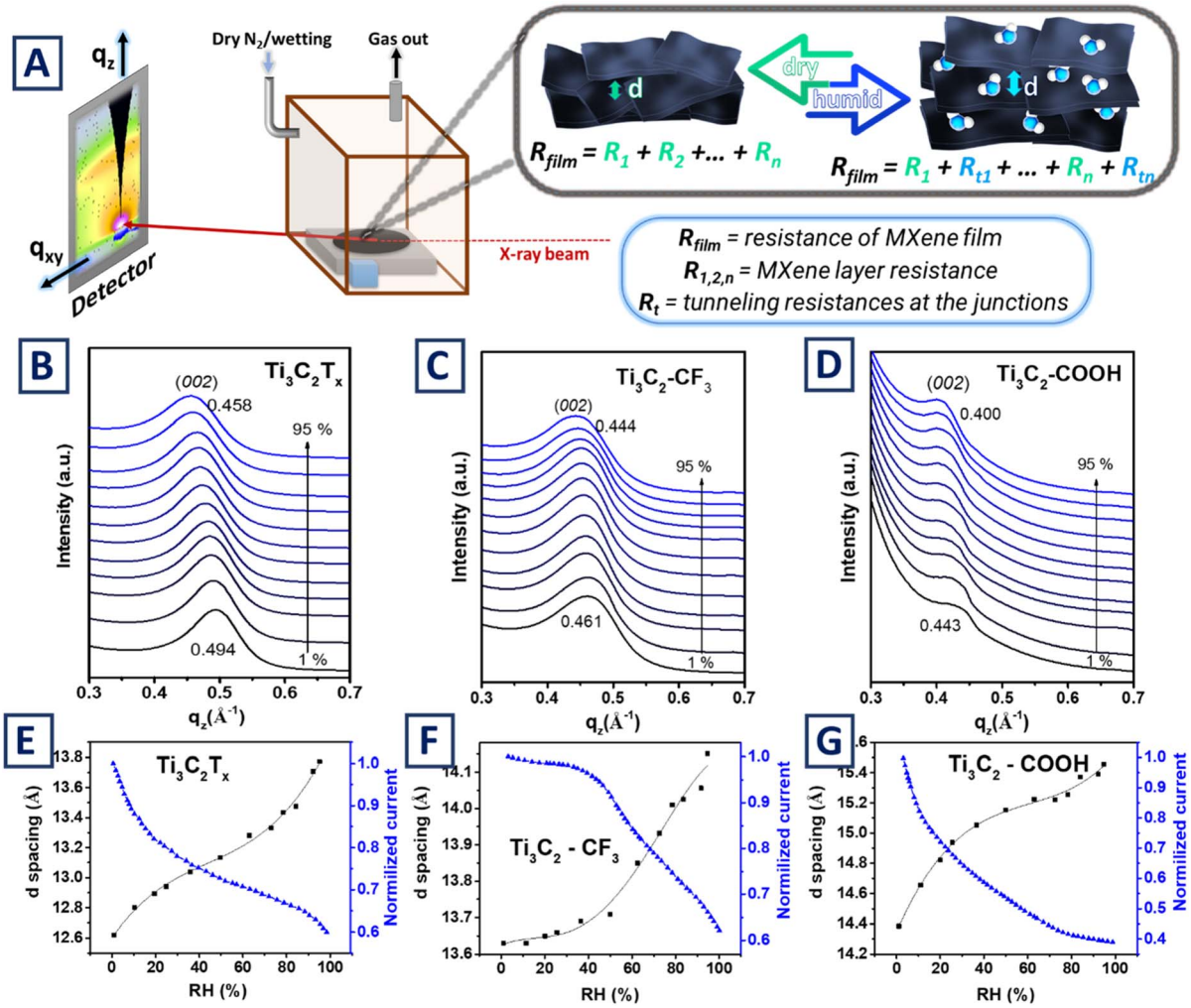

Fig. 4 (A) Schematic representation of GIWAXS *in situ* measurements of $Ti_3C_2T_x$ thin films response to humidity presence; (B)–(D) shifts of characteristic (002) XRD peak position of pristine and grafted $Ti_3C_2T_x$ films as a function of surrounding humidity level and flakes' surface terminations; (E)–(G) comparison of the changes of *d*-spacing of $Ti_3C_2T_x$ films and thin films conductivity changes, induced by the water molecules capture at different humidity levels.

formation of TiO_2. In particular, deconvolution of characteristic Ti peaks indicate the significant degree of TiO_2 formation after the pristine $Ti_3C_2T_x$ storage, while MXene grafting resulted in the suppression of TiO_2 formation. Thus, surface grafting not only increases the sensitivity of MXene-based sensor to particular humidity range (low humidity for Ti_3C_2–COOH and high humidity for of Ti_3C_2–CF_3 grafting) but also allows to increase the lifespan of the created sensor(s).

Finally, it should be noted again that the sensors based on 2D materials are currently an emerging topic. MXene-based sensors are useful because they match the required characteristics, such as low response time and high sensitivity.[15,16,60,61] Nevertheless, the sensors, including MXene based ones often have to combine multiple materials to improve their characteristics. One of the crucial drawbacks of humidity sensors is their inability to operate in the range of very low and high humidity (below 10% or above 90% humidity level). In this work, we tend to show how the inner parameters of MXene can be modified to extend its sensitivity range by means of surface modification (Fig. 3). Furthermore, the proposed covalent surface modification can also extend the lifetime of the sensor operation (Fig. 5D). In particular, we observed a significant increase in sensor resistivity (and a decrease in related functionality) only after 20 days of operation at 50 °C and a humidity level. Flakes degradation can be expected, since MXenes are relatively unstable materials (especially in the presence of water and oxygen, at increased temperature) and can undergo oxidation (with the formation of titanium oxide and carbon residues) after few weeks under ambient conditions.[39] However, the stability of the flakes can be significantly improved by immobilization of various chemical ligands on the surface of the flakes, including electrostatic grafting, hydrogen bonds, and the use of covalent grafting.[39,49,62–64] In our case, we also observed a significant increase in sensor stability due to previous surface grafting.

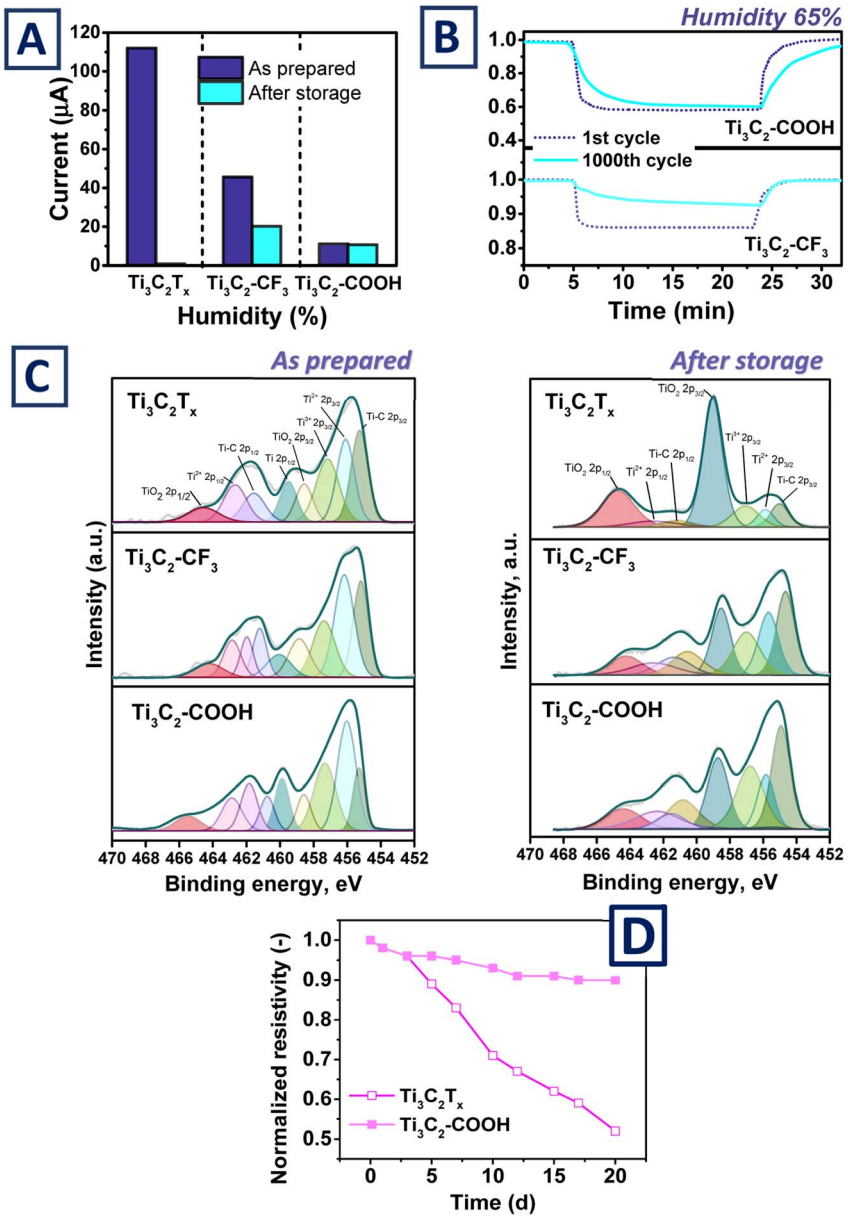

Fig. 5 (A) Conductance of pristine and grafted (*i.e.*, protected) $Ti_3C_2T_x$ films measured immediately after film deposition and after storage for 6 months at ambient conditions; (B) changes of grafted $Ti_3C_2T_x$ films response to humidity presence induced by flakes storage; (C) deconvolution of characteristic Ti 2p XPS peak, measured before and after storage of pristine and grafted $Ti_3C_2T_x$ thin films. (D) Estimation of sensor stability under operation conditions.

Conclusions

In conclusion, surface modification (surface termination tuning) of $Ti_3C_2T_x$ flakes was demonstrated along with the subsequent utilization of the obtained materials as an active material in humidity sensing. $Ti_3C_2T_x$ surface grafting was performed with the utilization of plasmon-assisted diazonium chemistry. Hydrophilic ($-C_6H_4-COOH$) and hydrophobic ($-C_6H_4-CF_3$) chemical groups were covalently grafted onto the flakes' surface, which significantly affects their interaction with water molecules. In particular, modification caused significant impact on the capture of water molecules and, accordingly, a humidity-induced increase of flakes' interlayer distance (after flakes arrangement in the form of thick films), which was confirmed by *in situ* GIWAXS measurements, performed at different humidity level with utilization of pristine and grafted flakes. The thin films created from flakes grafted with hydrophilic chemical moieties showed a better capture of water molecules and an increase in moisture sensing at low humidity levels, while the sensor grafted by $-C_6H_4-CF_3$ groups showed absence of water capturing at low humidity levels and effective capture of water molecules at high moisture concentrations, with corresponding increase of sensor sensitivity at high humidity levels. In addition, $Ti_3C_2T_x$ grafting significantly

increases the lifetime of MXenes films under ambient (and sensor operation) conditions, since the preliminary $Ti_3C_2T_x$ grafting inhibits the initial stages of flake oxidation and prevents formation of titanium oxide.

Author contributions

Vladislav Buravets – conceptualization, experimental and data curation. Anastasiia Olshtrem – methodology, investigation. Vasilii Burtsev – investigation. Gorin Oleg – investigation. Sergii Chertopalov – investigation, methodology, writing – review & editing. Andrei Chumakov – conceptualization, investigation. Matthias Schwartzkopf – conceptualization, investigation. Jan Lancok – methodology, validation. Vaclav Svorcik – validation, writing – review & editing. Oleksiy Lyutakov – methodology, writing – review & editing. Elena Miliutina – supervision; data curation, writing – original draft.

Conflicts of interest

There are no conflicts to declare.

Acknowledgements

This work was supported by the GACR under project No. 21-09277S. SC and JL acknowledge the Operational Program Research, Development and Education financed by European Structural and Investment Funds and the Czech Ministry of Education, Youth and Sports Project No. SOLID21 CZ.02.1.01/0.0/0.0/16_019/0000760. We acknowledge DESY (Hamburg, Germany), a member of the Helmholtz Association HGF, for the provision of experimental facilities. Parts of this research were carried out at PETRA III and we would like to thank P03 beamline staff for the assistance. Beamtime was allocated for proposal No. I-20230229 EC.

References

1 H. Tai, Z. Duan, Y. Wang, S. Wang and Y. Jiang, *ACS Appl. Mater. Interfaces*, 2020, **12**, 31037–31053.
2 H. Tai, S. Wang, Z. Duan and Y. Jiang, *Sens. Actuators, B*, 2020, **318**, 128104.
3 X. Zhou, Z. Xue, X. Chen, C. Huang, W. Bai, Z. Lu and T. Wang, *J. Mater. Chem. B*, 2020, **8**, 3231–3248.
4 B. Peng, F. Zhao, J. Ping and Y. Ying, *Small*, 2020, **16**, 2002681.
5 E. Owji, H. Mokhtari, F. Ostovari, B. Darazereshki and N. Shakiba, *Sci. Rep.*, 2021, **11**, 1771.
6 D. I. Petukhov, A. S. Kan, A. P. Chumakov, O. V. Konovalov, R. G. Valeev and A. A. Eliseev, *J. Membr. Sci.*, 2021, **621**, 118994.
7 V. Buravets, F. Hosek, L. Lapcak, E. Miliutina, P. Sajdl, R. Elashnikov, V. Švorčík and O. Lyutakov, *ACS Appl. Mater. Interfaces*, 2023, **15**, 5679–5686.
8 M. Naguib, O. Mashtalir, J. Carle, V. Presser, J. Lu, L. Hultman, Y. Gogotsi and M. W. Barsoum, *ACS Nano*, 2012, **6**, 1322–1331.
9 A. V. Mohammadi, J. Rosen and Y. Gogotsi, *Science*, 2021, **372**, eabf1581.
10 C. Wang, S. Chen and L. Song, *Adv. Funct. Mater.*, 2020, **30**, 2000869.
11 A. Zabelina, D. Zabelin, E. Miliutina, J. Lancok, V. Svorcik, S. Chertopalov and O. Lyutakov, *J. Mater. Chem. A*, 2021, **9**, 17770–17779.
12 B. Lu, Z. Zhu, B. Ma, W. Wang, R. Zhu and J. Zhang, *Small*, 2021, **17**, e2100946.
13 C. Zhang, Y. Luo, J. Tan, Q. Yu, F. Yang, Z. Zhang, L. Yang, H.-M. Cheng and B. Liu, *Nat. Commun.*, 2020, **11**, 3724.
14 Y. Gogotsi and Q. Huang, *ACS Nano*, 2021, **15**, 5775–5780.
15 H. Riazi, G. Taghizadeh and M. Soroush, *ACS Omega*, 2021, **6**, 11103–11112.
16 Y. Pei, X. Zhang, Z. Hui, J. Zhou, X. Huang, G. Sun and W. Huang, *ACS Nano*, 2021, **15**, 3996–4017.
17 S. J. Kim, H.-J. Koh, C. E. Ren, O. Kwon, K. Maleski, S.-Y. Cho, B. Anasori, C.-K. Kim, Y.-K. Choi, J. Kim, Y. Gogotsi and H.-T. Jung, *ACS Nano*, 2018, **12**, 986–993.
18 E. S. Muckley, M. Naguib, H.-W. Wang, L. Vlcek, N. C. Osti, R. L. Sacci, X. Sang, R. R. Unocic, Y. Xie, M. Tyagi, E. Mamontov, K. L. Page, P. R. C. Kent, J. Nanda and I. N. Ivanov, *ACS Nano*, 2017, **11**, 11118–11126.
19 M. Ghidiu, J. Halim, S. Kota, D. Bish, Y. Gogotsi and M. W. Barsoum, *Chem. Mater.*, 2016, **28**, 3507–3514.
20 E. S. Muckley, M. Naguib and I. N. Ivanov, *Nanoscale*, 2018, **10**, 21689–21695.
21 A. Lipatov, M. Alhabeb, M. R. Lukatskaya, A. Boson, Y. Gogotsi and A. Sinitskii, *Adv. Electron. Mater.*, 2016, **2**, 1600255.
22 C. J. Zhang, S. Pinilla, N. McEvoy, C. P. Cullen, B. Anasori, E. Long, S.-H. Park, A. Seral-Ascaso, A. Shmeliov, D. Krishnan, C. Morant, X. Liu, G. S. Duesberg, Y. Gogotsi and V. Nicolosi, *Chem. Mater.*, 2017, **29**, 4848–4856.
23 O. Salim, K. A. Mahmoud, K. K. Pant and R. K. Joshi, *Mater. Today Chem.*, 2019, **14**, 100191.
24 P. O. Å. Persson and J. Rosen, *Curr. Opin. Solid State Mater. Sci.*, 2019, **23**, 100774.
25 Y. Chae, S. J. Kim, S.-Y. Cho, J. Choi, K. Maleski, B.-J. Lee, H.-T. Jung, Y. Gogotsi, Y. Lee and C. W. Ahn, *Nanoscale*, 2019, **11**, 8387–8393.
26 S. Chertopalov and V. N. Mochalin, *ACS Nano*, 2018, **12**, 6109–6116.
27 S. Huang and V. N. Mochalin, *Inorg. Chem.*, 2019, **58**, 1958–1966.
28 R. Lotfi, M. Naguib, D. E. Yilmaz, J. Nanda and A. C. T. van Duin, *J. Mater. Chem. A*, 2018, **6**, 12733–12743.
29 F. Xia, J. Lao, R. Yu, X. Sang, J. Luo, Y. Li and J. Wu, *Nanoscale*, 2019, **11**, 23330–23337.
30 D. I. Petukhov, A. P. Chumakov, A. S. Kan, V. A. Lebedev, A. A. Eliseev, O. V. Konovalov and A. A. Eliseev, *Nanoscale*, 2019, **11**, 9980–9986.
31 R. A. Soomro, P. Zhang, B. Fan, Y. Wei and B. Xu, *Nano-Micro Lett.*, 2023, **15**, 108.
32 N. Liu, Q. Li, H. Wan, L. Chang, H. Wang, J. Fang, T. Ding, Q. Wen, L. Zhou and X. Xiao, *Nat. Commun.*, 2022, **13**, 5551.

33 H. Riazi, M. Anayee, K. Hantanasirisakul, A. A. Shamsabadi, B. Anasori, Y. Gogotsi and M. Soroush, *Adv. Mater. Interfaces*, 2020, **7**, 1902008.
34 V. Natu, J. L. Hart, M. Sokol, H. Chiang, M. L. Taheri and M. W. Barsoum, *Angew. Chem., Int. Ed.*, 2019, **58**, 12655–12660.
35 Y. Wang, J. Fu, J. Xu, H. Hu and D. Ho, *ACS Appl. Mater. Interfaces*, 2023, **15**, 12232–12239.
36 H. Bark, G. Thangavel, R. J. Liu, D. H. Chua and P. S. Lee, *Small Methods*, 2023, 2300077.
37 J. Swapnalin, B. Koneru, R. Pothu, P. Banerjee, R. Boddula, A. B. Radwan and R. Al-Qahtani, *Appl. Phys. Lett.*, 2023, **122**, 161902.
38 C. W. Wu, B. Unnikrishnan, I. W. P. Chen, S. G. Harroun, H. T. Chang and C. C. Huang, *Energy Storage Mater.*, 2020, **25**, 563–571.
39 T. Y. Ko, D. Kim, S. J. Kim, H. Kim, A. S. Nissimagoudar, S. C. Lee, X. Lin, P. T. Cummings, S. Doo, S. Park, T. Hassan, T. Oh, A. Chae, J. Lee, Y. Gogotsi, I. In and C. M. Koo, *ACS Nano*, 2023, **17**, 1112–1119.
40 H. Shin, H. Lee, Y. Seo, W. Jeong and T. H. Han, *Langmuir*, 2023, **39**, 2358–2367.
41 J. Yan, P. F. Liu, H. X. Wen and H. J. Liu, *ChemistrySelect*, 2022, **7**, e202201733.
42 Z. H. Liu, Q. M. Wang, Q. F. Lü and J. Wu, *Colloids Surf., A*, 2022, **640**, 128396.
43 M. Mozafari and M. Soroush, *Mater. Adv.*, 2021, **2**, 7277–7307.
44 L. Lorencova, V. Gajdosova, S. Hroncekova, T. Bertok, M. Jerigova, D. Velic, P. Sobolciak, I. Krupa, P. Kasak and J. Tkac, *Front. Chem.*, 2020, **8**, 553.
45 A. Popelka, A. C. Padmanabhan, A. S. Elgendy, P. Sobolciak, I. Krupa, A. B. Yousaf, M. Sebesta, J. Tkac and P. Kasak, *Mater. Today Commun.*, 2023, **35**, 105529.
46 Y. Fang, Z. Wei, Z. Guan, N. Shan, Y. Zhao, F. Liu, L. Fu, Z. Huang, M. G. Humphrey and C. Zhang, *J. Mater. Chem. C*, 2023, **11**, 7331–7344.
47 S. Bagheri, R. Chilcott, S. Luo and A. Sinitskii, *Langmuir*, 2022, **38**, 12924–12934.
48 A. N. Kumar and K. Pal, *Mater. Adv.*, 2022, **3**, 5151–5162.
49 V. Neubertova, O. Guselnikova, Y. Yamauchi, A. Olshtrem, S. Rimpelova, E. Čižmár, M. Orendáč, J. Duchon, L. Volfova, J. Lancok, V. Herynek, P. Fitl, P. Ulbrich, L. Jelinek, P. Schneider, J. Kosek, P. Postnikov, Z. Kolska, V. Svorcik, S. Chertopalov and O. Lyutakov, *Chem. Eng. J.*, 2022, **446**, 136939.
50 A. Olshtrem, S. Chertopalov, O. Guselnikova, R. R. Valiev, M. Cieslar, E. Miliutina, R. Elashnikov, P. Fitl, P. Postnikov, J. Lancok, V. Svorcik and O. Lyutakov, *2D Mater.*, 2021, **8**, 045037.
51 A. Olshtrem, I. Panov, S. Chertopalov, K. Zaruba, B. Vokata, P. Sajdl, J. Lancok, J. Storch, V. Církva, V. Svorcik, M. Kartau, A. S. Karimullah, J. Vana and O. Lyutakov, *Adv. Funct. Mater.*, 2023, **33**, 2212786.
52 E. A. Chernova, D. I. Petukhov, A. P. Chumakov, A. V. Kirianova, I. S. Sadilov, O. O. Kapitanova, O. V. Boytsova, R. G. Valeev, S. V. Roth, A. A. Eliseev and A. A. Eliseev, *Carbon*, 2021, **183**, 404–414.
53 A. Buffet, A. Rothkirch, R. Döhrmann, V. Körstgens, M. M. Abul Kashem, J. Perlich, G. Herzog, M. Schwartzkopf, R. Gehrke, P. Müller-Buschbaum and S. V. Roth, *J. Synchrotron Radiat.*, 2012, **19**, 647–653.
54 A. Sarycheva and Y. Gogotsi, *Chem. Mater.*, 2020, **32**, 3480–3488.
55 A. A. Eliseev, A. A. Poyarkov, E. A. Chernova, A. A. Eliseev, A. P. Chumakov, O. V. Konovalov and D. I. Petukhov, *2D Mater.*, 2019, **6**, 035039.
56 J.-C. Lei, X. Zhang and Z. Zhou, *Front. Phys.*, 2015, **10**, 276–286.
57 D. I. Petukhov, A. S. Kan, A. P. Chumakov, O. V. Konovalov, R. G. Valeev and A. A. Eliseev, *J. Membr. Sci.*, 2021, **621**, 118994.
58 C. Wu, A. C. Wang, W. Ding, H. Guo and Z. L. Wang, *Adv. Energy Mater.*, 2019, **9**, 1802906.
59 K. Dong, X. Peng and Z. L. Wang, *Adv. Mater.*, 2020, **32**, 1902549.
60 H. An, T. Habib, S. Shah, H. Gao, A. Patel, I. Echols, X. F. Zhao, M. Radovic, M. J. Green and J. L. Lutkenhaus, *ACS Appl. Nano Mater.*, 2019, **2**, 948–955.
61 N. Li, Y. Jiang, C. Zhou, Y. Xiao, B. Meng, Z. Wang, D. Huang, Ch. Xing and Z. Peng, *ACS Appl. Mater. Interfaces*, 2019, **11**, 38116–38125.
62 Y. Lee, S. Joon Kim, Y.-J. Kim, Y. Lim, Y. Chae, B.-J. Lee, Y.-T. Kim, H. Han, Y. Gogotsi and C. Won Ahn, *J. Mater. Chem. A*, 2020, **8**, 573–581.
63 S. Athavale, S. Micci-Barreca, K. Arole, V. Kotasthane, J. Blivin, H. Cao, J. L. Lutkenhaus, M. Radovic and M. J. Green, *Langmuir*, 2023, **39**, 918–928.
64 Z. Deng, L. Li, P. Tang, C. Jiao, Z. Z. Yu, C. M. Koo and H. B. Zhang, *ACS Nano*, 2022, **16**, 16976–16986.